scientific reports

Check for updates

OPEN

Rapid diagnosis of TERT promoter mutation using Terahertz absorption spectroscopy in glioblastoma

Zhiyan Sun[1,2], Minghui Du[1,2], Xianhao Wu[3], Rui Tao[1,2], Peiyuan Sun[1,2], Shaowen Zheng[3], Zhaohui Zhang[3,5], Dabiao Zhou[1,6]✉, Xiaoyan Zhao[3,4,6]✉ & Pei Yang[1,2,6]✉

Glioblastoma (GBM) is a highly aggressive brain tumor with poor outcomes and limited treatment options. The telomerase reverse transcriptase (TERT) promoter mutation, one of the key biomarkers in GBM, is linked to tumor progression and prognosis. This study employed terahertz time-domain spectroscopy (THz-TDS) to analyze frozen GBM tissue sections, extracting six spectral features: absorption coefficient, dielectric loss factor, dielectric constant, extinction coefficient, refractive index, and dielectric loss tangent. LASSO regression was employed for feature selection, and then principal component analysis (PCA) was applied to minimize inter-feature correlations. A Random Forest classifier built on these features successfully predicted TERT mutation status, achieving an area under the receiver operating characteristic curve (AUC) of 0.908 in the validation set. Our findings demonstrate that THz spectroscopy, coupled with machine learning, can identify molecular differences associated with TERT mutations, supporting its potential as a rapid, intraoperative diagnostic tool for personalized GBM treatment. This approach could enhance surgical decision-making and optimize patient outcomes through precise, real-time molecular diagnostics.

Keywords Terahertz, Glioblastoma, TERT, Machine learning, Biomarker identification

Glioblastoma (GBM) is the most common primary brain tumor in the adult central nervous system, characterized by rapid growth, high invasiveness, and a significant recurrence rate. Despite standard treatment protocols, including surgical resection, radiotherapy, and chemotherapy, the median survival remains approximately 15 months[1]. In 2016, the World Health Organization (WHO) incorporated molecular diagnostics into the classification of central nervous system (CNS) tumors for the first time[2]. The 2021 WHO classification further emphasized the role of molecular diagnostics, proposing that a definitive CNS tumor diagnosis must integrate both molecular markers and histopathological features. This shift marks a significant step towards more precise and personalized approaches to the diagnosis and treatment of GBM[3].

The TERT gene plays a crucial role in maintaining telomere length, which is essential for the proliferation of cancer cells[4]. Mutations in the promoter region of the TERT gene lead to its abnormal activation, driving the unlimited growth of tumor cells[5]. These promoter mutations are among the most frequent genetic alterations in GBM, found in approximately 70–80% of primary GBM cases[6–8]. The cIMPACT-NOW (Consortium to Inform Molecular and Practical Approaches to CNS Tumor Taxonomy) recommends using TERT promoter mutations as a key molecular marker to classify IDH-wildtype diffuse astrocytic gliomas with histological grades 2–3 as GBM, WHO grade IV[9]. This molecular marker reflects the aggressive nature of these tumors, equating them to glioblastomas in terms of prognosis and treatment, despite their lower histological grade. Simon, M. et al. demonstrated that TERT promoter mutations have a negative impact on the prognosis of patients with primary GBM, indicating that tumors with these mutations are more aggressive and prone to recurrence[6]. Additionally, TERT plays a crucial role in the molecular subtyping of gliomas. Among IDH-mutant gliomas, patients with

[1]Department of Neurosurgery, Beijing Tiantan Hospital, Capital Medical University, Beijing, China. [2]Beijing Neurosurgical Institute, Capital Medical University, Beijing, China. [3]School of Automation and Electrical Engineering, University of Science and Technology Beijing, Beijing, China. [4]Beijing Engineering Research Center of Industrial Spectrum Imaging, School of Automation and Electrical Engineering, University of Science and Technology Beijing, Beijing, China. [5]Shunde Innovation School, University of Science and Technology Beijing, Foshan, China. [6]These authors jointly supervised this work: Dabiao Zhou, Xiaoyan Zhao and Pei Yang. ✉email: dabiaozhou@163.com; zhaoxiaoyan@ustb.edu.cn; peiyang87@163.com

TERT mutations generally exhibit better prognosis compared to those with wild-type TERT. In contrast, in IDH-wildtype gliomas, TERT mutations are indicative of poor prognosis[10]. Consequently, detecting TERT promoter mutations is critical for understanding the biological behavior of the tumor, guiding clinical decisions, and improving patient outcomes. Currently, the clinical detection of TERT promoter mutations primarily relies on gene sequencing of tumor tissue after surgery[11], which typically takes around 10 days to yield a molecular pathology diagnosis. However, there is no rapid and accurate method available for intraoperative diagnosis of TERT mutations in glioblastoma. This delay in obtaining molecular diagnostic results limits the ability to make real-time surgical decisions based on the tumor's genetic profile.

Terahertz (THz) spectroscopy, a non-invasive and non-ionizing technique in the far-infrared region of the electromagnetic spectrum (0.1–10 THz), has gained increasing attention in biomedical research due to its ability to detect the unique vibrational and rotational modes of biomolecules[12]. Unlike traditional imaging and diagnostic methods, terahertz spectroscopy is highly sensitive to subtle changes in the dielectric properties of biological tissues, allowing for the rapid and precise differentiation of normal and tumor tissues by detecting variations in their absorption, refraction, and reflection characteristics[13]. Currently, the application of THz technology in gliomas is primarily focused on the delineation of tumor infiltration boundaries, differentiation between glioma grades, and the analysis of biophysical properties such as water content and cell density[14,15]. The extent of surgical resection is a critical factor for the prognosis of glioma patients. Studies have demonstrated that THz reflection imaging can effectively identify tumor boundaries in rat glioma models, with water content and tumor cell density being key contributors to these differences[16,17]. Young Bin Ji et al. further validated this approach in human gliomas of various grades[18]. THz time-domain reflection spectroscopy, which measures refractive index, has been used to detect both rat and human gliomas, with water content and cell density identified as the primary factors behind the refractive index variations[15,19]. Heterogeneity is a hallmark feature of gliomas. Kucheryavenko et al. applied solid immersion microscopy to detect intratumoral heterogeneity in rat glioma models, which was found to be associated with tumor cell accumulation, blood vessels, necrotic debris, and hemorrhage[20]. Ning Mu et al. used THz attenuated total reflection (ATR) time-domain spectroscopy to analyze human brain tumor tissues of different grades, and for the first time, they reported the ability to differentiate IDH-mutant and wild-type gliomas based on absorption coefficients[21]. However, the application of THz spectroscopy in predicting key molecular biomarkers in gliomas, such as TERT promoter mutations in glioblastoma (GBM), remains underexplored.

Machine learning algorithms play a crucial role in classifying tumor types and identifying specific molecular markers[22–24]. In this study, we incorporated multiple THz parameters, including absorption coefficient, refractive index, dielectric constant, extinction coefficient, dielectric loss factor, and dielectric loss tangent. By integrating machine learning, we successfully achieved the detection of TERT promoter mutations in GBM for the first time. Additionally, we discussed the factors underlying the differences in THz parameters between TERT-mutant and non-mutant gliomas. In summary, by combining THz time-domain spectroscopy (THz-TDS) with machine learning methods, we proposed a novel diagnostic approach for glioma molecular markers. This technique holds the potential for enabling rapid intraoperative diagnosis of TERT mutations in GBM, representing a significant advancement that could improve the accuracy and personalization of GBM treatment, ultimately enhancing patient prognosis.

Materials and methods

Tissue sample preparation

Fresh tumor specimens obtained intraoperatively were immediately placed in precooled phosphate-buffered saline (PBS) within an icebox and promptly transported to the laboratory for further processing. In the laboratory, the specimens were taken out of the PBS buffer, thoroughly blotted to eliminate surface moisture, and transferred into embedding molds. The frozen tissue-embedding agent (O.C.T., SAKURA, USA) was added to the molds, which were then left at 4 °C for 20–40 min to allow the O.C.T. to fully infiltrate the specimens. Subsequently, the samples were transferred to a -80 °C freezer and allowed to solidify completely before sectioning. Tumor tissues embedded in O.C.T. were sectioned using a YAMATO REM710 Slicing Machine, with the section thickness set to 100 μm and the cooling stage temperature maintained at -12 °C to preserve section integrity. The diameter of each section was set to at least 10 mm, ensuring it exceeded the terahertz beam spot size. Custom polyethylene (PE) sheet with a thickness of 2 mm were prepared as carriers, and the 100 μm tissue sections were evenly adhered to the PE films for terahertz measurement experiments.

All tissue samples used in this study were obtained from Beijing Tiantan Hospital, Capital Medical University. This study was approved by the Ethics Committee of Beijing Tiantan Hospital, and all methods were conducted in accordance with the relevant guidelines and regulations of the Ethics Committee of Beijing Tiantan Hospital, with written informed consent obtained from all patients. The inclusion criteria for patients were as follows: (a) diagnosed with glioblastoma (GBM, WHO grade IV) postoperatively according to the WHO 2021 classification; (b) TERT promoter mutation status determined by genetic sequencing; and (c) The tumor specimens are obtained, preserved, and sectioned strictly according to the conditions described in the previous paragraph. A total of 180 frozen sections from 9 GBM patients were obtained, including 40 sections with TERT promoter mutations and 140 sections without promoter mutations, as detailed in Supplementary Material 1.

Terahertz experimental setup scheme

In this study, terahertz time-domain spectroscopy was employed to characterize tissue sections, with the scanning path illustrated in Fig. 1. The femtosecond laser used (Toptica Photonics FemtoFErb) had a wavelength of 780 nm, a pulse duration of < 100 fs, and a laser power output of 15 mW. The terahertz frequency range utilized was 0.2–1.4 THz with a spectral resolution of 15 GHz. All optical components were mounted on a vibration isolation platform to minimize the impact of external environmental vibrations on the optical path.

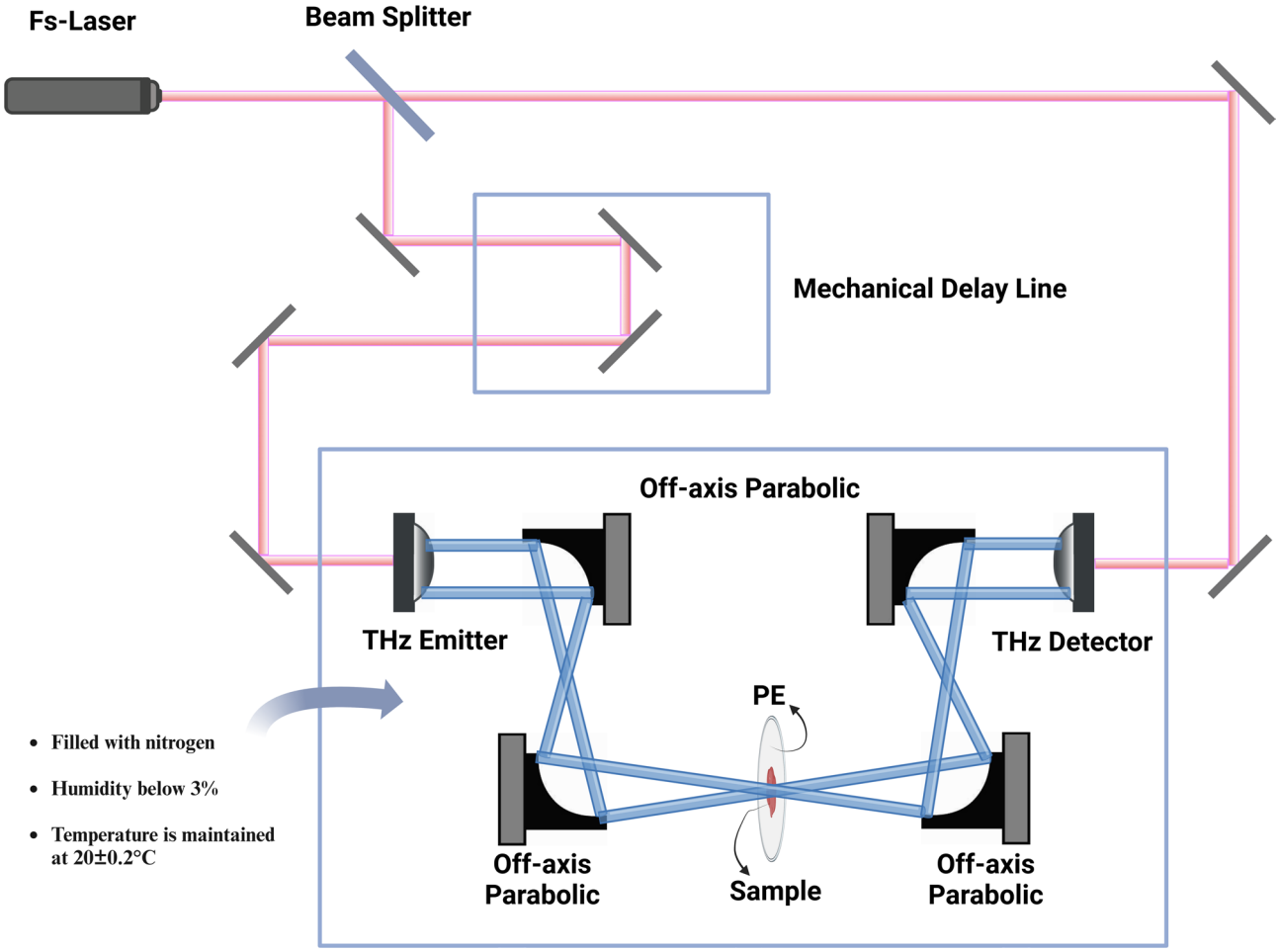

Fig. 1. Scan path diagram of the sample using terahertz time-domain spectroscopy. PE refers to polyethylene, which has very little absorption of terahertz waves and is a widely used biosample holder material in terahertz biological experiments.

Due to the strong absorption effect of water vapor on THz radiation, in order to minimize the impact of humidity fluctuations, the entire THz optical path was placed in a glass box filled with nitrogen. During testing, the relative humidity was maintained below 3%, and the temperature was kept at 20 °C ± 0.2 °C. To ensure a consistent testing environment within the same control group, a custom-made 6-well sample holder was used, where one reference sample (pure PE sheet) and five experimental samples (PE sheets with tissue samples) were placed (**Supplementary Fig. 1**). During the experiment, the samples were sequentially mounted on the porous rotating sample holder. Prior to measurement, to remove condensation formed on the sample surfaces when transferring from a frozen environment to room temperature, the samples were placed in an experimental chamber filled with flowing dry nitrogen for 15 min. During this process, the sample holder was rotated slowly to ensure even drying of the surface of each sample. The THz radiation spot had a diameter of approximately 5 mm. At the beginning of the measurement, the sample position was adjusted to align the center of the pure PE sheet with the focal point of the THz spot, and the reference signal was recorded. The sample holder was then rotated 60 degrees each time to ensure that the sample remained precisely positioned at the focus of the THz radiation, allowing for the subsequent measurement of 5 additional sets of sample signals. For each set, data were collected three times and averaged to reduce errors. We measured the frozen tumor sections and got six terahertz parameters, including the absorption coefficient, dielectric loss factor, dielectric constant, extinction coefficient, refractive index, and dielectric loss tangent. Data transformation and the related formulas are provided in **Supplementary Material 2**. Further specific details can be found in our previous studies[25,26].

The processing of Terahertz data and the development of diagnostic models

The dataset comprising 180 tissue sections characterized by THz spectroscopy was randomly divided into a training set with 125 samples and a validation set with 55 samples. Lasso regression was applied to the training set for THz features selection, and an ROC curve was plotted for each selected terahertz feature. Principal component analysis (PCA) was then employed to reduce correlations among the selected features. A Random Forest model was constructed based on the reduced features from the training set. Finally, the predictive

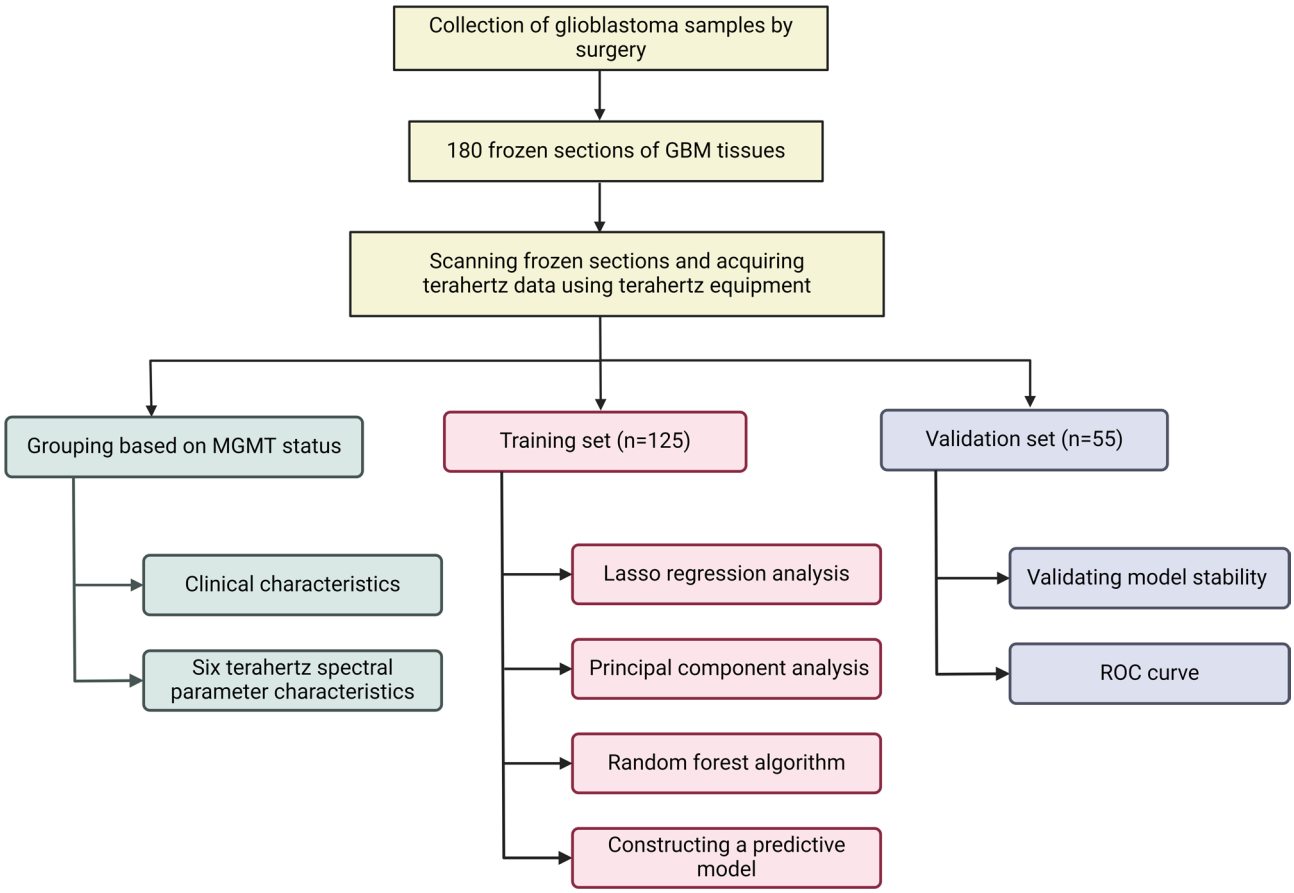

Fig. 2. Workflow diagram of the modeling process.

Group	Mean age (years)	Sex (male/female)	TERT_mut (yes/no)
Training set ($N=125$)	51.8	83/42	29/96
Validation set ($N=55$)	51.4	37/18	11/44
P-value	0.84	1.00	0.78

Table 1. Detailed information of 180 tissue sections.

performance of the model was evaluated in the validation set using ROC curves. The detailed workflow is shown in Fig. 2.

Statistical analysis

Data analysis was performed using R software (version 4.4.1). Terahertz spectral feature selection was conducted using the Lasso algorithm from the "glmnet" package, while PCA was applied using the "stats" package to reduce correlations among the selected features. A Random Forest model was constructed using the "randomForest" package, and ROC curves were plotted using the "pROC" package. Frequency plots of the THz features were generated using Python 3.8. A P-value of less than 0.05 was considered statistically significant.

Result

Clinical characteristics of the training and validation sets

We performed a statistical analysis of the age, gender, and TERT promoter mutation status for the 125 tissue samples in the training set and the 55 tissue samples in the validation set. Age was assessed using the t-test, with a p-value of 0.84. Gender and TERT promoter mutation status were evaluated using the chi-square test, with p-values of 1.00 and 0.78, respectively (Table 1). The results showed no significant differences in age, gender, or TERT promoter mutation status between the two groups, indicating that the classification results are reliable.

Different Terahertz parameters in mutated and non-mutated States of the Tert promoter

We analyzed 6 THz parameters, including αs(ω) (absorption coefficient), εi(ω) (dielectric loss factor), εr(ω) (dielectric constant), κs(ω) (extinction coefficient), ns(ω) (refractive index), and tanδ (dielectric loss tangent),

to compare the differences between samples with different TERT mutation statuses within the 0.2–1.4 THz frequency range. The results showed significant differences in the dielectric constant and refractive index between samples with different TERT mutation statuses, while the other parameters did not exhibit statistically significant differences (Fig. 3).

Extraction of Terahertz feature parameters

Each of the 6 THz parameters—refractive index, absorption coefficient, extinction coefficient, dielectric constant, dielectric loss factor, and dielectric loss tangent—has 82 values within the 0.2–1.4 THz frequency range, resulting in a total of 492 THz feature parameters. Since these 6 terahertz parameters can be interconverted, there is inherent correlation among different parameters at the same THz frequency, necessitating data redundancy reduction. The Lasso regression algorithm, by introducing a penalty coefficient, effectively selects important features, eliminating redundancy, controlling model complexity, and enhancing the model's generalizability[27]. We used the Lasso regression algorithm with 10-fold cross-validation repeated 2000 times, determining the optimal penalty coefficient λ (λ = 0.00470). This allowed us to filter the 492 THz feature parameters and ultimately identify 14 highly correlated THz features (Fig. 4), with detailed feature information provided in Table 2. The 14 selected THz features were individually used to predict the TERT promoter mutation status of the samples. The model's performance was evaluated using ROC curves, and the results indicated that all AUC values were below 0.8, suggesting that the predictive performance of the model was suboptimal (Fig. 5A-N).

Modeling and validation

We performed a Spearman correlation analysis on the 14 THz spectral features obtained from the Lasso regression algorithm and found strong correlations between some of the features (Fig. 6A). Principal component analysis (PCA) is a method that transforms the original features into a new set of linearly independent variables (principal components) to reduce multicollinearity among features[28]. By applying PCA, we reduced the degree of association among the 14 features while preserving most of the original information, thereby improving the model's accuracy and stability. After PCA, we performed a new Spearman correlation analysis on the processed data, revealing a significant reduction in feature correlations (Fig. 6B). The Mean Decrease Accuracy and Mean Decrease Gini metrics indicated that PC11 and PC10 were the most important principal components for the Random Forest (RF) model, as they made substantial contributions to both model accuracy and data segmentation (Fig. 6C). Using the training set, we built a prediction model based on the 14 principal components (PCs) with the RF algorithm. The model's predictive ability was assessed using ROC curves, showing a specificity of 1 and a sensitivity of 0.75, with an AUC of 0.908 (Fig. 6D). Additionally, the F1-score, Precision-Recall curves, and calibration plots further demonstrate the stability and reliability of the model (**Supplementary Fig. 2**). These results indicate that the predictive model performs exceptionally well in predicting the TERT promoter mutation status in GBM.

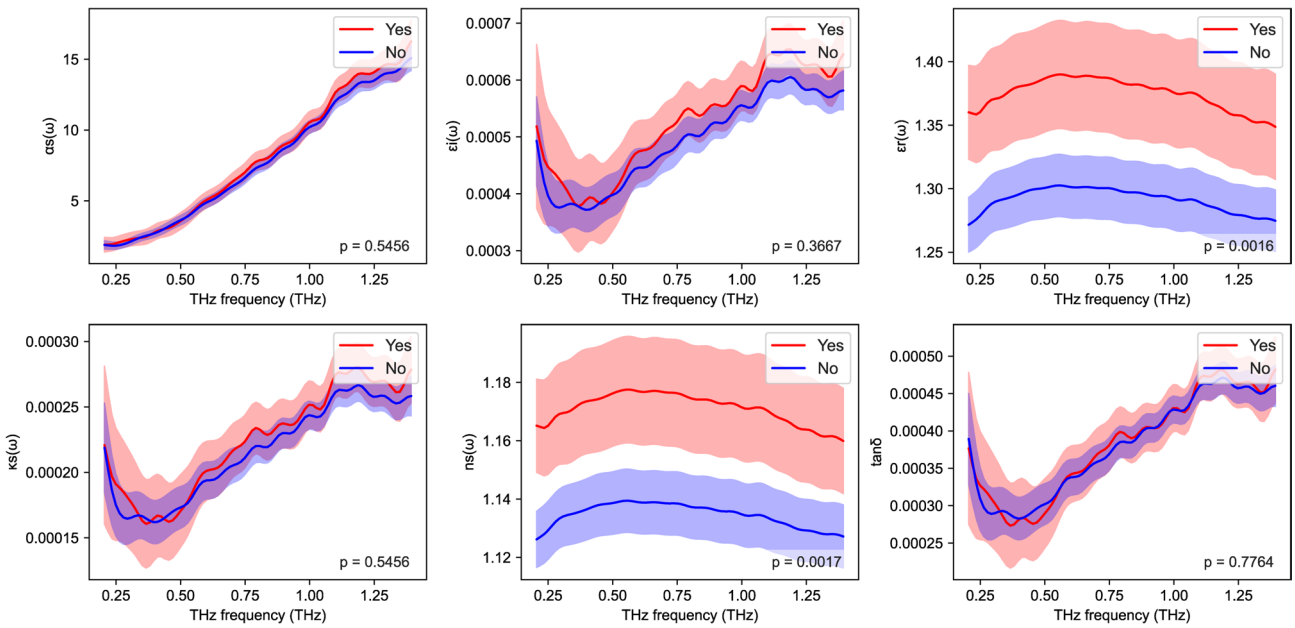

Fig. 3. Terahertz frequency curves of different terahertz parameters based on Tert promoter mutation status. *Given that the integration of Lasso, PCA, and RF can eliminate redundancies, retain the most discriminative features, effectively model nonlinear relationships, and enhance model performance, we utilized machine learning methodologies for model construction rather than direct classification using single indicators such as refractive index values.

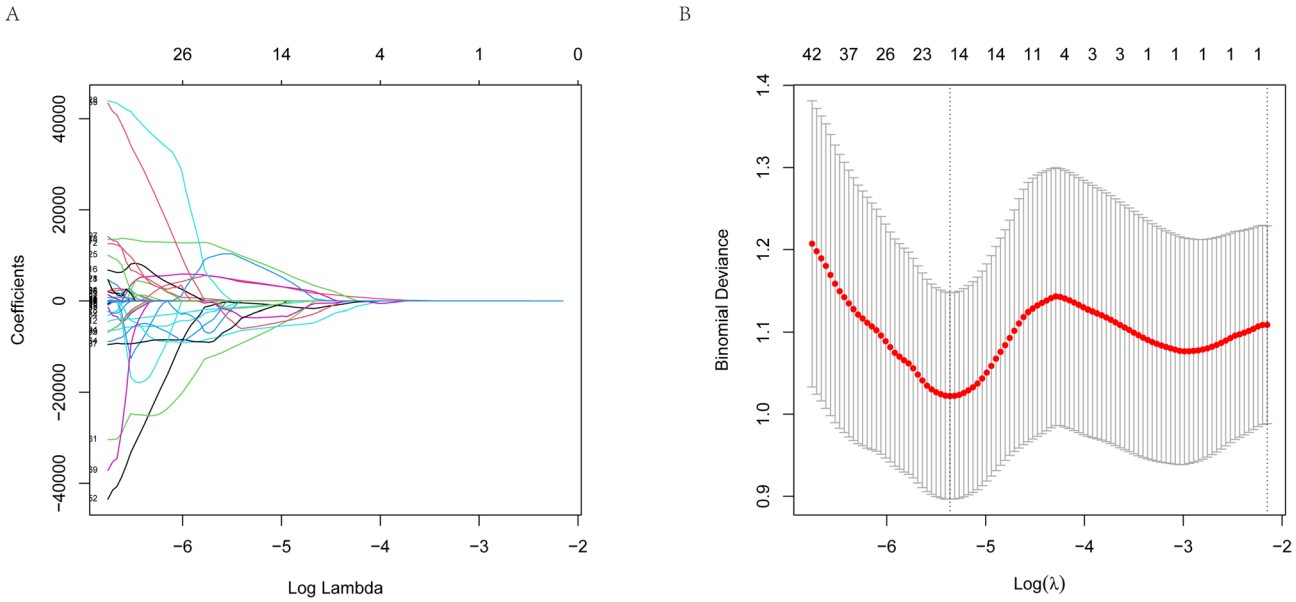

Fig. 4. Feature selection based on the Lasso algorithm.

Feature name	Feature type	THz frequency
293.3 GHz_εi(ω)	Dielectric loss factor	0.2933 THz
410.6 GHz_εi(ω)	Dielectric loss factor	0.4106 THz
718.5 GHz_εi(ω)	Dielectric loss factor	0.7185 THz
1217.0 GHz_εi(ω)	Dielectric loss factor	1.2170 THz
1349.0 GHz_εi(ω)	Dielectric loss factor	1.3490 THz
1393.0 GHz_εr(ω)	Dielectric constant	1.3930 THz
205.3 GHz_ns(w)	Refractive index	0.2053 THz
220.0 GHz_tanδ	Dielectric loss tangent	0.2200 THz
366.6 GHz_tanδ	Dielectric loss tangent	0.3660 THz
469.2 GHz_ tanδ	Dielectric loss tangent	0.4692 THz
571.9 GHz_tanδ	Dielectric loss tangent	0.5719 THz
586.5 GHz_tanδ	Dielectric loss tangent	0.5865 THz
967.8 GHz_tanδ	Dielectric loss tangent	0.9678 THz
1393.0 GHz_tanδ	Dielectric loss tangent	1.3930 THz

Table 2. 14 Terahertz signatures screened by lasso.

Discussion

Our findings show that samples with TERT promoter mutations exhibit higher refractive index and dielectric constant compared to non-mutated samples. Materials with a high dielectric constant typically demonstrate stronger refractive effects on light, indicating a positive correlation between the refractive index and dielectric constant. As the dielectric constant increases, the refractive index also increases[29]. TERT promoter mutations lead to increased TERT expression, which functions to extend telomeres, allowing cells to evade replicative senescence and maintain unlimited proliferative capacity[30]. This mutation is commonly associated with the highly malignant characteristics of glioblastoma[31]. Rapidly proliferating tumor cell populations generally have higher cell density[32] and greater metabolic activity. For example, studies by Viswanath et al. demonstrated enhanced glucose metabolism via the pentose phosphate pathway (PPP) in TERT promoter-mutated gliomas[33], and Ahmad et al. found that lipid metabolism was upregulated in GBM cells with TERT promoter mutations[34]. These increases in cellular membranes and intracellular components likely contribute to the enhanced dielectric response of tissues in the terahertz frequency range. Changes in cell density and internal structure may lead to the observed increase in dielectric constant, which, in turn, results in an increased refractive index. Meng et al.'s study demonstrated that gliomas exhibit higher dielectric constant, refractive index, and absorption coefficient compared to normal tissues[35]. However, in our study, no significant differences were observed in the absorption coefficient between TERT-mutant and non-mutant GBM. This discrepancy may be due to the dominant role of water in absorbing electromagnetic waves, as the water content in both TERT-mutant and non-mutant GBM

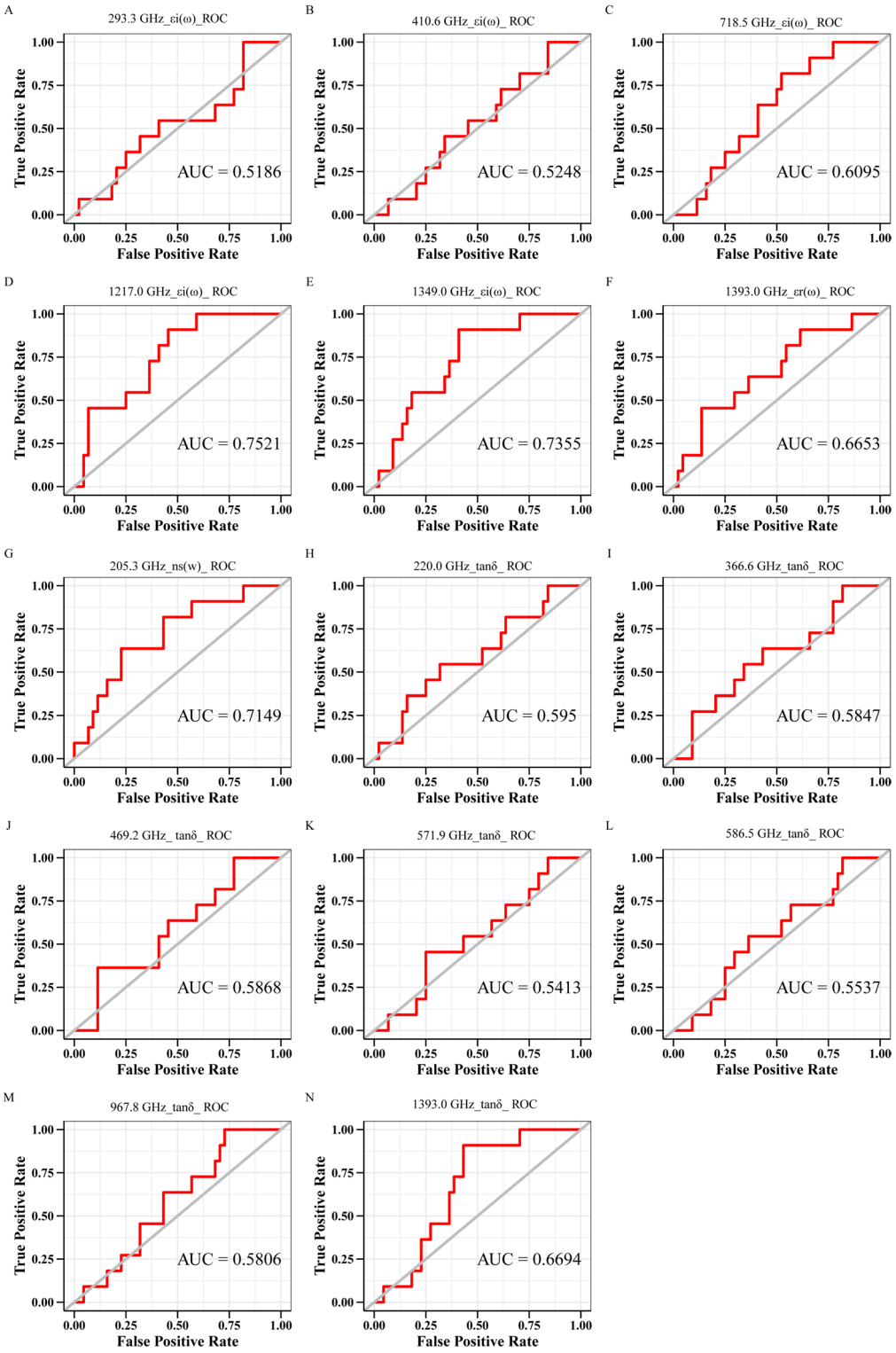

Fig. 5. (**A**–**N**) ROC curves for each feature.

tumor tissues is similar. The absorption characteristics of water may mask the influence of other molecular or tissue properties on the absorption coefficient.

THz spectroscopy can distinguish gliomas from normal tissue during surgery and rapidly identify unclear tumor margins without the need for labeling, thus facilitating complete tumor resection[36,37]. Moreover, Ning Mu and colleagues effectively distinguished between IDH-mutant and wild-type gliomas using THz spectral features. Our team further combined THz spectral features with machine learning algorithms to construct a model for predicting IDH mutation status in glioblastoma, achieving an AUC of 0.844[25]. As a molecular marker,

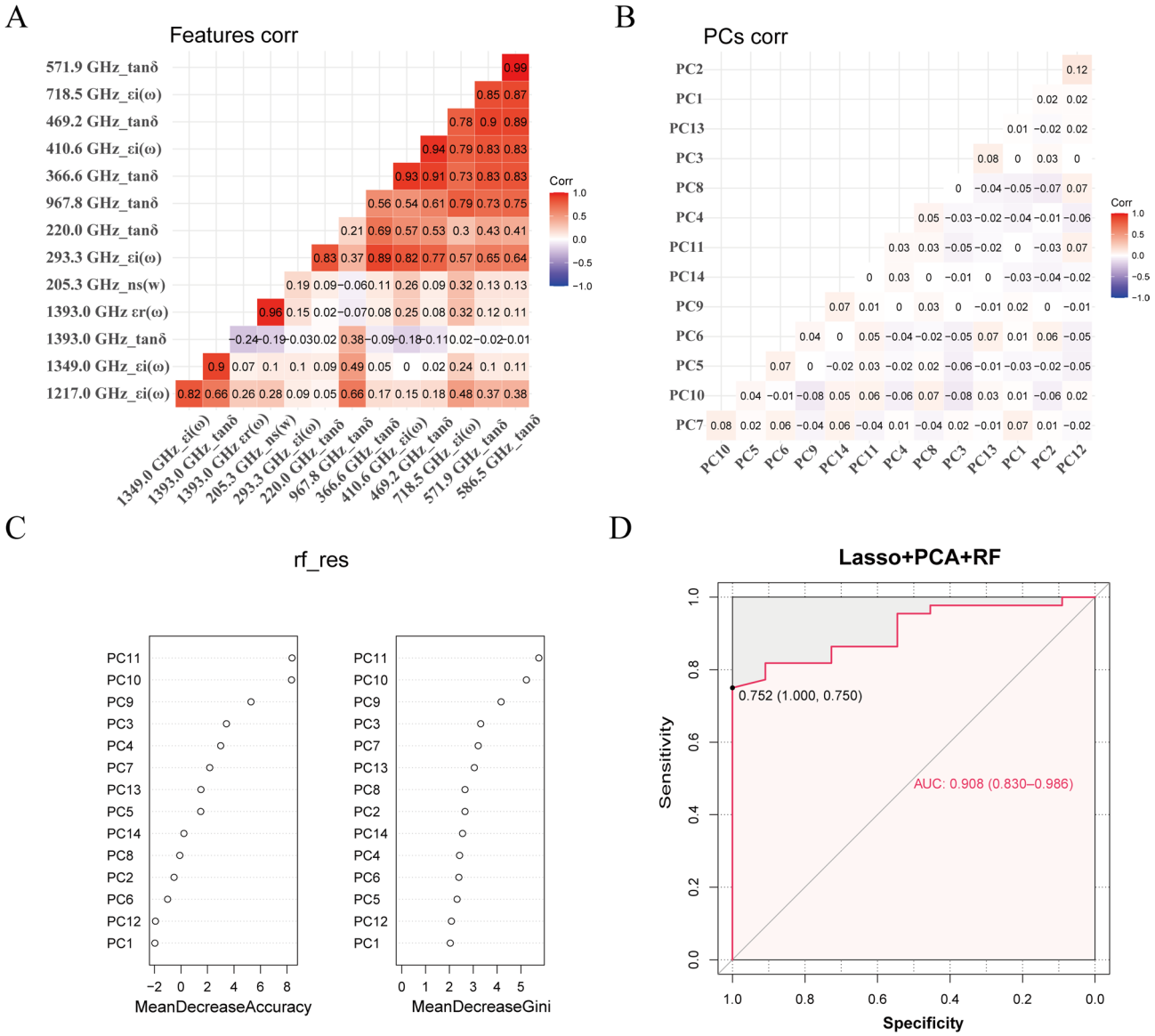

Fig. 6. (**A**) Correlation map of 14 terahertz parameter features (**B**) Correlation map of 14 terahertz parameter features after PCA (**C**) Plots of feature importance ranking (**D**) ROC curve of the predictive model.

TERT mutation has been widely applied in the molecular classification and prognostic evaluation of gliomas. In this study, we used THz spectral features from frozen sections of glioblastoma. We performed feature selection using the Lasso algorithm to identify 14 key THz parameters and applied PCA to reduce correlations among these features. Using the resulting parameters, we constructed a Random Forest-based prediction model for TERT promoter mutation status, achieving an AUC of 0.908, which demonstrated excellent predictive performance. Maarten R. Grootendorst et al. utilized THz spectroscopy with a handheld TPI probe system to differentiate between benign and malignant breast tissues and assess resection margins, achieving an accuracy of 75%, sensitivity of 86%, and specificity of 66%[38]. In the future, combining preoperative radiomics-based molecular marker prediction models with intraoperative molecular marker prediction models for glioblastoma may enhance the accuracy of GBM molecular marker predictions. Additionally, developing a portable handheld detection system could facilitate rapid intraoperative clinical diagnosis.

The earlier the pathological results of gliomas are confirmed, the more favorable it is for accurate diagnosis and clinical treatment. Terahertz technology has the potential to be applied intraoperatively to guide the complete resection of the infiltrative margins of gliomas. After collecting terahertz data from the samples, it could be integrated with various molecular prediction models (e.g., IDH, TERT, EGFR) to rapidly assess the molecular pathology of gliomas, thereby enabling a comprehensive intraoperative diagnosis of glioma pathology. This approach holds great promise for significantly improving diagnostic efficiency and reducing errors associated with variability in pathologist expertise. Currently, intraoperative pathological confirmation primarily relies on frozen section analysis. Although this method has a relatively short processing time, the rapid preparation of frozen sections often results in poor preservation of tissue morphology, which can lead

to decreased diagnostic accuracy and greater dependence on the skill of the pathologist. Additionally, it does not provide molecular pathological information, such as the status of TERT promoter mutations[39]. The clinical gold standard for glioma diagnosis combines postoperative histopathological analysis with molecular pathology based on gene sequencing. However, this process is time-consuming, often requiring up to two weeks post-surgery to confirm TERT mutation status. Such delays can hinder timely clinical decision-making, including intraoperative adjustments to achieve more extensive tumor resection in cases of higher-grade gliomas indicated by molecular pathology and the initiation of postoperative radiotherapy and chemotherapy at an earlier stage. Exploratory technologies that have not yet been widely adopted in clinical practice include intraoperative PCR and radiomics-based prediction of glioma molecular markers. Intraoperative rapid detection based on PCR technology is limited by its ability to assess only a single molecular characteristic, thus failing to provide a comprehensive evaluation of the tumor's molecular profile. The detection process, which still takes approximately one hour, may extend the overall duration of surgery. Additionally, this method cannot identify the specific type of tumor, rendering it inadequate for distinguishing between tumors that are difficult to differentiate on preoperative MRI, such as lymphoma and glioma[40–42]. Radiomics models based on MRI characteristics can predict TERT promoter mutation status in GBM preoperatively, with AUC values greater than 0.9, making them suitable for preoperative assessment and long-term follow-up, but they cannot provide real-time intraoperative monitoring[43–45].

Although our model demonstrated good performance in predicting TERT promoter mutations, the relatively small sample size may limit the generalizability of the findings. Larger and more diverse cohorts are needed to confirm the model's robustness across different patient populations. Furthermore, the use of more advanced machine learning algorithms could enhance the model's accuracy and stability. It is also important to note that the application of terahertz spectroscopy in biological tissues is still in its early stages. The relationship between these spectral features and the underlying molecular mechanisms of TERT promoter mutations remains unclear, which may limit our biological interpretation of the predictive outcomes.

Conclusion

This study employed a terahertz time-domain spectroscopy system to measure terahertz parameters in the frequency range of 0.2–1.4 THz, including absorption coefficient, dielectric loss factor, dielectric constant, extinction coefficient, refractive index, and dielectric loss tangent, yielding a total of 492 terahertz feature parameters. Through Lasso regression, 14 key terahertz feature parameters were selected, and PCA was applied to reduce correlations among these features. A prediction model for TERT promoter mutations was constructed based on these 14 features using the Random Forest algorithm in the training set. Validation of the model in the validation set using the ROC curve yielded an AUC of 0.908, demonstrating the model's excellent predictive capability. This model holds promising potential for precise molecular diagnostics of GBM and intraoperative clinical decision-making.

Data availability

Data are available from the corresponding authors upon request.

Received: 16 December 2024; Accepted: 19 May 2025
Published online: 27 May 2025

References

1. Stupp, R. et al. Radiotherapy plus concomitant and adjuvant Temozolomide for glioblastoma. *N. Engl. J. Med.* **352**, 987–996. https://doi.org/10.1056/NEJMoa043330 (2005).
2. Louis, D. N. et al. The 2016 world health organization classification of tumors of the central nervous system: a summary. *Acta Neuropathol.* **131**, 803–820. https://doi.org/10.1007/s00401-016-1545-1 (2016).
3. Louis, D. N. et al. The 2021 WHO classification of tumors of the central nervous system: a summary. *Neuro-oncology* 23, 1231–1251 (2021). https://doi.org/10.1093/neuonc/noab106
4. Killela, P. J. et al. TERT promoter mutations occur frequently in gliomas and a subset of tumors derived from cells with low rates of self-renewal. *Proc. Natl. Acad. Sci. U.S.A.* **110**, 6021–6026. https://doi.org/10.1073/pnas.1303607110 (2013).
5. Roake, C. M. & Artandi, S. E. Regulation of human telomerase in homeostasis and disease. *Nat. Rev. Mol. Cell Biol.* **21**, 384–397. https://doi.org/10.1038/s41580-020-0234-z (2020).
6. Simon, M. et al. TERT promoter mutations: a novel independent prognostic factor in primary glioblastomas. *NEURO-ONCOLOGY* **17**, 45–52. https://doi.org/10.1093/neuonc/nou158 (2015).
7. Nguyen, H. N. et al. Human TERT promoter mutation enables survival advantage from MGMT promoter methylation in IDH1 wild-type primary glioblastoma treated by standard chemoradiotherapy. *NEURO-ONCOLOGY* **19**, 394–404. https://doi.org/10.1093/neuonc/now189 (2017).
8. Arita, H. et al. Upregulating mutations in the TERT promoter commonly occur in adult malignant gliomas and are strongly associated with total 1p19q loss. *Acta Neuropathol.* **126**, 267–276. https://doi.org/10.1007/s00401-013-1141-6 (2013).
9. Fujimoto, K. et al. TERT promoter mutation status is necessary and sufficient to diagnose IDH-wildtype diffuse astrocytic glioma with molecular features of glioblastoma. *Acta Neuropathol.* **142**, 323–338. https://doi.org/10.1007/s00401-021-02337-9 (2021).
10. Eckel-Passow, J. E. et al. Glioma groups based on 1p/19q, IDH, and TERT promoter mutations in tumors. *N. Engl. J. Med.* **372**, 2499–2508. https://doi.org/10.1056/NEJMoa1407279 (2015).
11. Penkova, A. et al. Comprehensive clinical assays for molecular diagnostics of gliomas: the current state and future prospects. *Front. Mol. Biosci.* **10** https://doi.org/10.3389/fmolb.2023.1216102 (2023).
12. Yang, X. et al. Biomedical applications of Terahertz spectroscopy and imaging. *Trends Biotechnol.* **34**, 810–824. https://doi.org/10.1016/j.tibtech.2016.04.008 (2016).
13. Cong, M. Y. et al. Biomedical application of Terahertz imaging technology: a narrative review. *Quant. IMAGING Med. Surg.* **13**, 8768–8786. https://doi.org/10.21037/qims-23-526 (2023).
14. Chernomyrdin, N. V. et al. Terahertz technology in intraoperative neurodiagnostics: A review. *OPTO-ELECTRONIC Adv.* **6** https://doi.org/10.29026/oea.2023.220071 (2023).

15. Gavdush, A. A. et al. Terahertz spectroscopy of gelatin-embedded human brain gliomas of different grades: a road toward intraoperative THz diagnosis. *J. Biomed. Opt.* **24** https://doi.org/10.1117/1.JBO.24.2.027001 (2019).
16. Oh, S. J. et al. Study of freshly excised brain tissues using Terahertz imaging. *BIOMEDICAL Opt. EXPRESS.* **5**, 2837–2842. https://doi.org/10.1364/BOE.5.002837 (2014).
17. Yamaguchi, S. et al. Brain tumor imaging of rat fresh tissue using Terahertz spectroscopy. *Sci. Rep.* **6** https://doi.org/10.1038/srep30124 (2016).
18. Ji, B. Terahertz reflectometry imaging for low and high grade gliomas. *Sci. Rep.* **6** https://doi.org/10.1038/srep36040 (2016).
19. Yamaguchi, S. et al. Origin and quantification of differences between normal and tumor tissues observed by Terahertz spectroscopy. *Phys. Med. Biol.* **61**, 6808–6820. https://doi.org/10.1088/0031-9155/61/18/6808 (2016).
20. Kucheryavenko, A. S. et al. Terahertz dielectric spectroscopy and solid immersion microscopy of ex vivo glioma model 101.8: brain tissue heterogeneity. *BIOMEDICAL Opt. EXPRESS.* **12**, 5272–5289. https://doi.org/10.1364/BOE.432758 (2021).
21. Mu, N. et al. Molecular pathological recognition of freshly excised human glioma using Terahertz ATR spectroscopy. *BIOMEDICAL Opt. EXPRESS.* **13**, 222–236. https://doi.org/10.1364/BOE.445111 (2022).
22. Shi, J. et al. Automatic evaluation of traumatic brain injury based on Terahertz imaging with machine learning. *Opt. Express.* **26**, 6371–6381. https://doi.org/10.1364/OE.26.006371 (2018).
23. Cho, H. H., Lee, S. H., Kim, J. & Park, H. Classification of the glioma grading using radiomics analysis. *PEERJ* **6** https://doi.org/10.7717/peerj.5982 (2018).
24. De Looze, C. et al. Machine learning: a useful radiological adjunct in determination of a newly diagnosed glioma's grade and IDH status. *J. Neurooncol.* **139**, 491–499. https://doi.org/10.1007/s11060-018-2895-4 (2018).
25. Sun, Z. Y. et al. Prediction of IDH mutation status of glioma based on Terahertz spectral data. *SPECTROCHIMICA ACTA PART. A-MOLECULAR Biomol. Spectrosc.* **295** https://doi.org/10.1016/j.saa.2023.122629 (2023).
26. Wu, X. H. et al. Biomedical applications of Terahertz spectra in clinical and molecular pathology of human glioma. *SPECTROCHIMICA ACTA PART. A-MOLECULAR Biomol. Spectrosc.* **285** https://doi.org/10.1016/j.saa.2022.121933 (2023).
27. Tibshirani, R. Regression shrinkage and selection via the Lasso. *J. ROYAL Stat. Soc. Ser. B-STATISTICAL Methodol.* **58**, 267–288. https://doi.org/10.1111/j.2517-6161.1996.tb02080.x (1996).
28. Jolliffe, I. T. & Cadima, J. Principal component analysis: a review and recent developments. *PHILOSOPHICAL TRANSACTIONS OF THE ROYAL SOCIETY A-MATHEMATICAL PHYSICAL AND ENGINEERING SCIENCES* 374 (2016). https://doi.org/10.1098/rsta.2015.0202
29. Grigorev, R. O., Khodzitsky, M. K., Zhang, T. & Demchenko, P. S. in *OPTICS IN HEALTH CARE AND BIOMEDICAL OPTICS VIII* Vol. 10820 (2018).
30. vanSteensel, B. & deLange, T. Control of telomere length by the human telomeric protein TRF1. *NATURE* **385**, 740–743. https://doi.org/10.1038/385740a0 (1997).
31. Killela, P. J. et al. Mutations in IDH1, IDH2, and in the TERT promoter define clinically distinct subgroups of adult malignant gliomas. *ONCOTARGET* **5**, 1515–1525. https://doi.org/10.18632/oncotarget.1765 (2014).
32. Sabelström, H. et al. High density is a property of slow-cycling and treatment-resistant human glioblastoma cells. *Exp. Cell Res.* **378**, 76–86. https://doi.org/10.1016/j.yexcr.2019.03.003 (2019).
33. Viswanath, P. et al. Metabolic imaging detects elevated glucose flux through the Pentose phosphate pathway associated with TERT expression in low-grade gliomas. *NEURO-ONCOLOGY* **23**, 1509–1522. https://doi.org/10.1093/neuonc/noab093 (2021).
34. Ahmad, F. et al. Telomerase reverse transcriptase (TERT) - enhancer of Zeste homolog 2 (EZH2) network regulates lipid metabolism and DNA damage responses in glioblastoma. *J. Neurochem.* **143**, 671–683. https://doi.org/10.1111/jnc.14152 (2017).
35. Meng, K. et al. Terahertz pulsed spectroscopy of paraffin-embedded brain glioma. *J. Biomed. Opt.* **19** https://doi.org/10.1117/1.JBO.19.7.077001 (2014).
36. Wu, L. M. et al. Study of in vivo brain glioma in a mouse model using continuous-wave Terahertz reflection imaging. *BIOMEDICAL Opt. EXPRESS.* **10**, 3953–3962. https://doi.org/10.1364/BOE.10.003953 (2019).
37. Cherkasova, O. et al. Diagnosis of glioma molecular markers by Terahertz technologies. *PHOTONICS* **8** https://doi.org/10.3390/photonics8010022 (2021).
38. Grootendorst, M. R. et al. Use of a handheld Terahertz pulsed imaging device to differentiate benign and malignant breast tissue. *BIOMEDICAL Opt. EXPRESS.* **8**, 2932–2945. https://doi.org/10.1364/BOE.8.002932 (2017).
39. Kurdi, M. et al. Diagnostic discrepancies between intraoperative frozen section and permanent histopathological diagnosis of brain tumors. *TURKISH J. Pathol.* **38**, 34–39. https://doi.org/10.5146/tjpath.2021.01551 (2022).
40. Diplas, B. H. et al. Sensitive and rapid detection of TERT promoter and IDH mutations in diffuse gliomas. *NEURO-ONCOLOGY* **21**, 440–450. https://doi.org/10.1093/neuonc/noy167 (2019).
41. Li, J. et al. Intraoperative rapid molecular diagnosis aids glioma subtyping and guides precise surgical resection. *Ann. Clin. Transl. Neurol.* **11**, 2176–2187. https://doi.org/10.1002/acn3.52138 (2024).
42. Shankar, G. M. et al. Rapid intraoperative molecular characterization of glioma. *JAMA Oncol.* **1**, 662–667. https://doi.org/10.1001/jamaoncol.2015.0917 (2015).
43. Chen, L. et al. MRI radiomics model for predicting TERT promoter mutation status in glioblastoma. *BRAIN Behav.* **13** https://doi.org/10.1002/brb3.3324 (2023).
44. Zhang, H. B. et al. Peritumoral radiomics for identification of telomerase reverse transcriptase promoter mutation in patients with glioblastoma based on preoperative MRI. *CANADIAN ASSOCIATION OF RADIOLOGISTS JOURNAL-JOURNAL DE L ASSOCIATION CANADIENNE DES RADIOLOGISTES* **75**, 143–152 (2024). https://doi.org/10.1177/08465371231183309
45. Zhang, H. B. et al. Deep learning radiomics for the assessment of telomerase reverse transcriptase promoter mutation status in patients with glioblastoma using multiparametric MRI. *J. Magn. Reson. Imaging.* **58**, 1441–1451. https://doi.org/10.1002/jmri.28671 (2023).

Acknowledgements

The authors thank all individuals who participated in this study and donated samples. We sincerely thank the Department of Pathology at Beijing Tiantan Hospital for providing the pathological diagnoses. Additionally, Figure 1 was created in BioRender. Du, M. (2025) https://BioRender.com/c10r443.

Author contributions

Writing-Original Draft: M.H.D.; Writing-Review & Editing: M.H.D. and Z.Y.S.; Conceptualization: M.H.D. and Z.Y.S.; Methodology: Z.Y.S., R.T., P.Y. and X.Y.Z.; Investigation: X.H.W, P.Y.S, S.W.Z, and Z.H.Z.; Funding Acquisition: P.Y., D.B.Z and Z.Y.S.; Resources: P.Y and X.Y.Z.; Supervision: P.Y., D.B.Z and X.Y.Z.

Funding

This work was supported by the Beijing Municipal Administration of Hospitals Incubating Program (PX2024019), the Postdoctoral Fellowship Program of CPSF (GZC20231749), the National Natural Science Foundation of

China (82151310), the Beijing Natural Science Foundation (L246018) and Beijing Municipal Natural Science Foundation (7254342).

Declarations

Competing interests
The authors declare no competing interests.

Additional information
Supplementary Information The online version contains supplementary material available at https://doi.org/10.1038/s41598-025-03161-x.

Correspondence and requests for materials should be addressed to D.Z., X.Z. or P.Y.